Process Safety and Environmental Protection 170 (2023) 1079–1091

Contents lists available at ScienceDirect

Process Safety and Environmental Protection

journal homepage: www.journals.elsevier.com/process-safety-and-environmental-protection

Green synthesis of reduced graphene oxide and their use on column adsorption of phenol from olive mill wastewater

Imane Haydari [a,b], Khalid Aziz [c], Savaş Kaya [d], Taner Daştan [e], Naaila Ouazzani [a,b], Laila Mandi [a,b], Faissal Aziz [a,b,*]

[a] Laboratory of Water, Biodiversity, and Climate Change, Faculty of Sciences Semlalia, Cadi Ayyad University, BP 2390, 40000 Marrakech, Morocco
[b] National Center for Research and Studies on Water and Energy (CNEREE), Cadi Ayyad University, B. 511, 40000 Marrakech, Morocco
[c] Laboratory of Materials and Environment, Faculty of Sciences, Ibn Zohr University, BP 8106, Agadir 80000, Morocco
[d] Sivas Cumhuriyet University, Health Services Vocational School, Department of Pharmacy, 58140 Sivas, Turkey
[e] Sivas Cumhuriyet University, Faculty of Science, Department of Biochemistry, 58140 Sivas, Turkey

ARTICLE INFO

Keywords:
Adsorption
Green synthesis
Reduced graphene oxide
Phenol
Verbena officinalis

ABSTRACT

A novel reduced graphene oxide (RGO) synthesis using *Verbena officinalis* as a green, reducing agent was outreaching. RGO was encapsulated in sodium alginate (SA) by cross-linking (SA-RGO beads). SA-RGO beads have been used to treat olive mill wastewater (OMWW). This effluent is rich in phenolic compounds that inhibit biological degradation and are toxic at high concentrations. The newly prepared SA-RGO beads were characterized by scanning electron microscopy (SEM),energy-dispersive X-ray spectroscopy (EDS), X-ray diffractometer (XRD), BET surface area analyzer, and Fourier transforms infrared spectroscopy (FTIR). In addition, the organic compounds of *Verbena officinalis* were determined by HPLC to reveal the reduction mechanism of graphene oxide (GO). Finally, batch and fixed-bed column adsorption tests were performed to assess the performance of SA-RGO beads. The kinetics, isotherm models and adsorption thermodynamics show that the pseudo-second-order and Freundlich best present phenol adsorption and the endothermic reaction. Thomas and Yoon-Nelson's models satisfactorily described fixed-bed column adsorption. The optimized adsorption parameters were 3.68 g L^{-1} of adsorbent dosage, pH of 4.0, adsorption time of 135 min, and temperature of 25 °C. The reusability of SA-RGO beads and regeneration experiments with HCl (0.5 M) were performed in fixed-bed reactors. The results showed a phenol adsorption capacity of 994 mg g^{-1} for an initial concentration of 4000 mg L^{-1}.

1. Introduction

The olive sector is an important industry, especially in the Mediterranean region. However, olive oil production gives large amounts of by-products, including olive pomace (30 %) and olive mill wastewater (OMWW), with negative environmental effects (Duarte et al., 2014; Atallah et al., 2019a; Ayeda et al., 2019).

OMWW is an environmental pollutant characterized by its strong high turbidity, unpleasant odor, acidic pH and high chemical oxygen demand (COD = 3500–85,000 mg L^{-1}) (Lissaneddine et al., 2021). In addition, this effluent contains many organic materials, such as organic acid, phenolic compounds ranging from 600 to 25,000 mg L^{-1}, polysaccharides, etc (Ioannou-Ttofa et al., 2017; Atallah et al., 2019a). Phenolic pollutants are classified by the U.S. Environmental Protection Agency (USEPA) as priority pollutants because of their acute toxicity, bio-recalcitrant nature, and toxic effects on animals and humans and remain in the aquatic environment over a very long period. In addition, phenolic compounds regularly enter water bodies from domestic, agricultural and industrial activities. Therefore, phenolic compounds such as phenols and chlorophenols have been classified as toxic phenolic pollutants (Kilic et al., 2019; Coskun et al., 2010; Rout and Jena, 2022).

Many techniques have been applied to recover phenolic molecules from OMWW, particularly electrolysis, chromatography, membrane system and extraction methods (Ceccon et al., 2001; Paraskeva et al., 2007). However, some of these methods show disadvantages in high cost and low toxicity reduction (Zaharaki and Komnitsas, 2018; Atallah et al., 2019a). Generally, the adsorption method is considered a promising method for wastewater treatment because it has many advantages

* Corresponding author at: Laboratory of Water, Biodiversity, and Climate Change, Faculty of Sciences Semlalia, Cadi Ayyad University, BP 2390, 40000 Marrakech, Morocco.
E-mail address: f.aziz@uca.ma (F. Aziz).

https://doi.org/10.1016/j.psep.2022.12.086
Received 31 October 2022; Received in revised form 22 December 2022; Accepted 30 December 2022
Available online 2 January 2023

over other methods, such as cost-effectiveness, high removal efficiency, insensitivity to toxic pollutants, operational and design simplicity, application flexibility and non-toxic end products (Rout and Jena, 2022; Sun et al., 2019; Aziz et al., 2020).

Several adsorbents are applied to recover phenol from the wastewater, including carbon sorbents, polymer matrix composites, and mineral zeolites (Aly et al., 2018; Ververi and Goula, 2019; Vavouraki et al., 2020). Carbon-based adsorbents, such as graphene, are the most effective material due to their large surface area, chemical stability, abundant active sites, and low cost. In addition, graphene has a two-dimensional carbon nanostructure with sp^2 bonding and a C═C conjugate ring structure (Geim and Novoselov, 2007).

Currently, research is focused on reduced graphene oxide (RGO) instead of graphene due to its strong chemical interaction, surface area, porosity and pH, etc. The reduced graphene oxide structure has graphitic domains containing residual oxygen functionalities, defect sites and π-electronic domains; all its properties allow the capacity of RGO as a sorbent for wastewater treatment containing organic molecules (Gupta and Khatri, 2017). The common method for graphene oxide (GO) reduction is chemical exfoliation by oxidation of graphite and the GO reduction mechanism (El Din Mahmoud, 2020). Many chemical reducing agents have been employed, such as hydroquinone ($C_6H_6O_2$), sodium borohydride ($NaBH_4$), di-methylhydrazine ($C_2H_8N_2$), hydrazine (N_2H_4-H_2O) and hydrogen sulfide (H_2S). However, these reducing agents are toxic and dangerous to humans and the environment (Weng et al., 2019). Therefore, environmentally friendly reduction processes are applied using green reducers extracted from the plant as they are non-toxic and low-cost. In addition, extracts from plant material can reduce GO due to the presence of various photochemical compounds. This study used *Verbena officinalis* leaf extract for GO reduction for the first time.

Generally, due to the low granulometry of adsorbents, their use in the fixed-bed column process has some drawbacks, such as the problem of bed compaction and an increase in the pressure drop. To overcome these disadvantages, their encapsulation with alginate-based hydrogels is an intriguing approach that has proven useful in continuous treatment (Aziz et al., 2020). Many studies currently use beads with alginate coatings on various adsorbents to be more effective and applicable for phenolic compound removal (Lissaneddine et al., 2021). Nadavala et al. (2009) used chitosan with calcium alginate mixed composite beads; Duarte et al. (2014) studied silica-alginate-fungus biocomposites. Kim et al. (2008) used alginate beads with activated carbon, and Jodra and Mijangos (2003) prepared composite beads based on calcium alginate. This work is the first study on the combined use of reduced graphene oxide with sodium alginate for the sorption of phenol from OMWW.

This work aims to monitor the effectiveness of composite beads prepared from graphene oxide reduced by *Verbena officinalis* as an eco-friendly sorbent for treating the OMWW. FTIR, SEM, EDS, and XRD characterized the prepared beads. Adsorption parameters of phenol on SA-RGO beads were studied, such as contact time, initial concentration and pH. In addition, the adsorption isotherm models, kinetic models and thermodynamic parameters are studied. The adsorption tests in a fixed-bed reactor were performed, and Kinetic models were used to analyze the adsorption process. Finally, HCl regeneration was performed to assess the reusability of SA-RGO beads in a fixed-bed column.

2. Materials and methods

2.1. Materials

OMWW treated in this work was collected in the Marrakech-Safi region of Morocco. Fresh OMWW samples were taken from extraction in a three-phases process and then stored at 20 °C. Sigma-Aldrich provided all chemicals applied in this study.

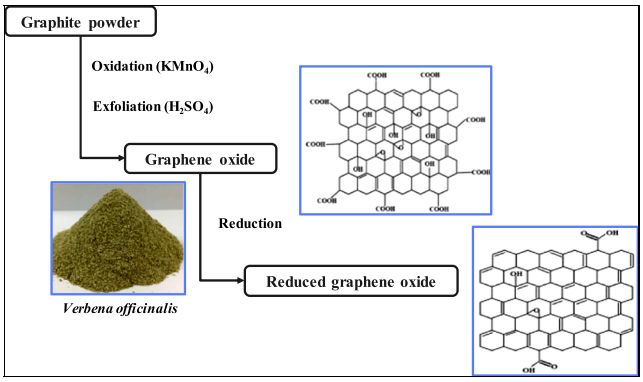

Fig. 1. Representation' steps of the preparation of RGO.

2.2. Physic-chemical characterization of OMWW

A Hanna HI 9829 probe determined the pH and electrical conductivity measurements. According to the standard, AFNOR T 90-101 determined the chemical oxygen demand (COD) in an acidic and warm environment by oxidation with potassium dichromate. Sulfate, nitrite, Kjeldahl nitrogen, nitrate and total phosphorus were estimated according to AFNOR T90-023, AFNOR T90-013, AFNOR T90-110, RODIER (1984), and AFNOR T90-022, respectively. Caffeic acid was used as a standard in the Folin-Ciocalteu method for estimating phenol concentration (Singleton and Rossi, 1965).

2.3. Preparation of GO

GO was prepared from graphite by applying the modified Hummer method (Aunkor et al., 2016). The detailed procedure followed a quantity of 1 g of graphite powder was intermingled with 25 mL of sulfuric acid (H_2SO_4) and a mass of 0.5 of sodium nitrate ($NaNO_3$) was added to the solution, then a slow addition of 3 g of potassium permanganate ($KMnO_4$) in 2 h. The mixture was stirred into an ice bath. The solution was kept for 2 h at a temperature of 35 °C. Next, 50 mL of distilled water was poured into the solution slowly under stirring and at a temperature of 95 °C for 30 min, followed by the direct addition of 400 mL of distilled water. Next, 5 mL of hydrogen peroxide 30 % (H_2O_2) was

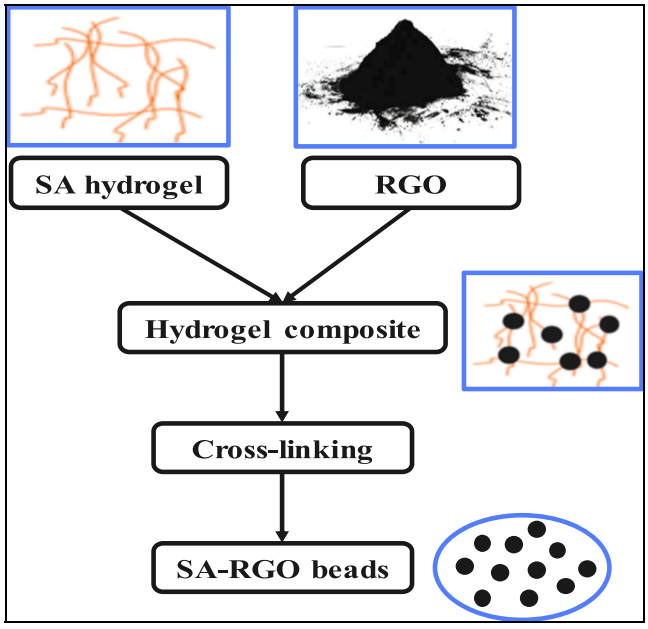

Fig. 2. A schematic representation of the preparation of SA–RGO beads.

added slowly under vigorous stirring. The GO was centrifuged and washed with distilled water and hydrochloric acid (HCl) 0.5 N. Finally, the GO powder was air-dried.

2.4. Green synthesis of RGO using extracts from Verbena officinalis

The aqueous extract of *Verbena officinalis* was prepared using the plant leaves (2 g). First, they were surface cleaned with running water and added 20 mL of 60 °C distilled water for 5 min. This extract was filtered by Millipore filter (0.45 μm). First, 100 mg of GO was mixed with distilled water (100 mL), then 12 mL of *Verbena officinalis* extract solution was added. Next, the suspension was stirred for 3 h at 25 °C. After reduction, the suspension was centrifuged at 3000 rpm. A reduced graphene oxide (RGO) was thus obtained and washed with distilled water several times and air-dried. Fig. 1 shows the RGO preparation steps.

2.5. Preparation of the SA-RGO beads

The SA-RGO beads preparation has been done following the cross-linking process (Fig. 2). First, an immediate solution of the sodium hydrogel alginate (2 %) at 30 °C was prepared. Then, a homogeneous dispersion was prepared under stirring (2 h) by mixing RGO powder (2 %) with alginate. Finally, the solidification of the beads consisted of pouring the secondary mixture into a calcium chloride ($CaCl_2$) 20 % cross-linking solution. The resulting SA-RGO beads were washed water and stored in ultrapure water.

2.6. Characterization of SA-RGO beads

Fourier transform infrared spectroscopy was used to examine the chemical functions in RGO and SA-RGO beads using KBr pellets in a 65 spectrum of ALPHA-P, Germany, in the frequency range from 400 to 4000 cm^{-1}. The physicochemical characteristics of the SA-RGO beads were studied using XRD. Morphological characteristics of SA-RGO beads and RGO were determined by scanning electron microscopy (JSM-5900LV, Japan). The pHPZC (point of zero charges) was determined by Lopez-Ramon et al. (1999). This method consists in introducing a quantity of SA-RGO beads in the phenol solution (25 mL) at various initial pH, under agitation (3 h) at a temperature of 25 °C. The BET method was used to calculate the specific surface area (SBET) and the total volume (VT) of SA-RGO beads that had been previously outgassed and assessed by nitrogen adsorption at − 196 °C (via a Micromeritics ASAP 2020 surface analyzer system). The average pore radius (r^-) was calculated from (Eq. (1)) (Lawal et al., 2020):

$$r^- \ (nm) = \left(\frac{2V_T}{S_{BET}}\right) \times 10^3 \tag{1}$$

2.7. UHPLC of Verbeinea officinalis

HPLC analysis was used to detect *Verbeinea officinalis* elements. The analysis was performed in an Ultimate 3000 (Dionex, CA, USA), consisting of a sample changer (WPS 3000 TSL), a quaternary pump (HPG 3400 RS), and a column oven (TCC 3000). This method used a reverse phase column with the following dimensions 250 × 4.6 mm, particle size 2.6 μm (CA, USA). Gradient separation using solvent A (formic acid solution 0.1 %) and solvent B (methanol) was performed according to the protocol of Zefzoufi et al. (2021). Chromatographic profiles were performed in a 280 nm wavelength and UV-Vis spectra were recorded in the 200–400 nm range.

2.8. Adsorption studies

2.8.1. Batch adsorption

For batch adsorption, a mass of SA-RGO beads (4 g) was mixed with a volume of 25 mL of phenol solution in 50 mL conical flasks under stirring at 200 rpm for the equilibration time. To determine the phenol concentration, samples were taken from the flasks every 15 min. After the kinetic experiments, the impact of concentration (10, 30, 100, 300, 700, 1000, 2000, 3000 and 4000 mg L^{-1}) and pH (2, 4, 6, 8, 10, and 12) on the phenol adsorption process on SA-RGO beads was examined. The pH adjustment is made either by HCl (0.1 M) or NaOH (0.1 M).

The adsorption capacity was determined according to equation (Eq. (2)):

$$q = \frac{(C_0 - C_t)}{m} V \tag{2}$$

where, C_o is the initial concentration (mg L^{-1}), C_t is the concentration after a certain time of contact with SA-RGO beads (mg L^{-1}), V is the volume of phenol solution (L) and m is the amount of SA-RGO beads (g).

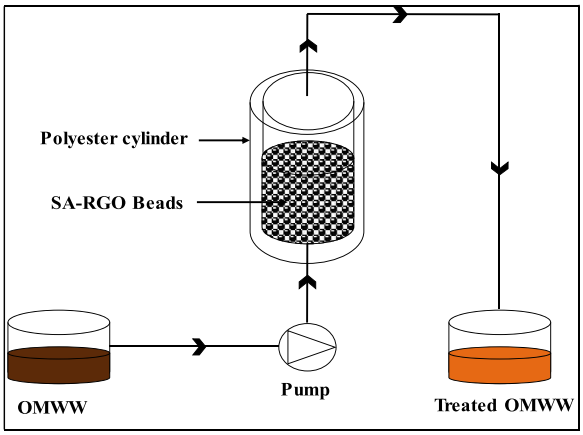

Fig. 3. Fixed-bed column implementation.

Table 1
Freundlich and Langmuir Isotherm.

Isotherm model	Equation	Eq. no.	Ref.
Freundlich	$logq_e = \log K_F + \frac{1}{n}\log C_e$	(3)	(Freundlich, 1906)
Langmuir	$\frac{C_e}{q_e} = \frac{C_e}{q_m} + \frac{1}{K_L q_m}$	(4)	(Langmuir, 1916)

C_e the equilibrium concentration of phenol (mg L^{-1}); q_m the maximum adsorption capacity (mg g^{-1}); q_e the equilibrium adsorbed amount (mg g^{-1}); K_L the Langmuir isothermal constant (L mg^{-1}); n adsorption intensity.

2.8.2. Column experiments

The fixed-bed column tests were performed through a column of 0.5 cm in diameter and 50 cm in height. Fig. 3 shows the implementation of the fixed-bed column. First, breakthrough curves were plotted every 15 min for 150 min until saturation of the SA-RGO beads sites. Different process parameters at which the column study was performed were the flow rates of real effluent of OMWW (0.5, 1.5 and 3 mL min^{-1}) and the height of the SA-RGO beads (Z = 15, 25 and 35 cm). The results were then subjected to linear regression analysis of Adams-Bohart, Thomas, Wol-borska, and Yoon-Nelson kinetic models to determine the fit of the experimental data to the models used. Next, OMWW was pumped into the column using a peristaltic pump (Fig. 3).

2.8.3. Batch and fixed-bed column data analysis

2.8.3.1. Dynamic batch adsorption models. Langmuir and Freundlich's adsorption isotherm models were applied in this study to explain the adsorption phenomena of phenol on SA-RGO beads. Table 1 presents the equations of the isotherm models.

Table 2
Pseudo-frst-order, Pseudo-second-order, and intra-particle diffusion kinetic models equations.

Kinetic model	Equation	Eq. no.	Ref.
Pseudo-frst-order	$\ln(q_e - q_t) = lnq_e - K_1 t$	(5)	(Subramanyam and Das, 2009)
Pseudo-second-order	$\frac{t}{q_t} = \frac{1}{K_2 q_e^2} + \frac{t}{q_e}$	(6)	(Subramanyam and Das, 2009)
Intra-particle Diffusion	$q_t = K_{id} t^{0.5} + C$	(7)	(Weber et al., 1963)

q_t adsorption capacity at each time point (mg g^{-1}); K_1 pseudo-first-order kinetic model rate constant (min^{-1}); K_2 pseudo-second-order kinetic model rate constant (g mg^{-1} min^{-1}); K_{id} (mg^{-1} $min^{-1/2}$) the intra-particle diffusion rate constant and C (mg g^{-1}) is a constant defining the boundary layer thickness.

Pseudo-first-order, pseudo-second-order, and intra-particle diffusion kinetic models were used in the experimental results to explain the adsorption of phenol. The equations of the kinetic models are given in Table 2.

Thermodynamic studies have been conducted to determine whether an adsorption mechanism is exothermic, endothermic, or spontaneous. The standard entropy ΔS° (J mol^{-1} K^{-1}) change, gibbs energy ΔG° (kJ mol^{-1}), and standard enthalpy ΔH° (kJ mol^{-1}) change, K_C is the thermodynamic distribution coefficient (Table 3).

2.8.3.2. Dynamic column adsorption kinetics models. Four kinetic models were applied to explain the experimental results: Adams-Bo-hart, Thomas, Wol-borska and Yoon-Nelson. The linear form of the equations is presented in Table 4. The root mean square error (RMSE) analysis was performed to firm up the best kinetic model (Eq. (12)).

$$RMSE = \sqrt[2]{\frac{1}{n}\sum\left(y_{pred} - y_{exp}\right)^2} \quad (12)$$

Table 3
Thermodynamic parameters.

Equation	Eq. no.
$\Delta G = -RT\ln K_c$	(8)
$\Delta G = \Delta H^0 - T\Delta S^0$	(9)
$\ln K_c = -\frac{\Delta H}{RT} + \frac{\Delta S}{R}$	(10)
$K_c = \frac{q_e}{C_e}$	(11)

Table 4
Adams-Bo-hart, Thomas, Wol-borska and Yoon-Nelson kinetics models equations.

Model	Equation	Eq. no.	Ref.
Adams-Bohart	$\ln\frac{C_t}{C_0} = K_{AB}C_0 t - K_{AB}N_0\frac{Z}{U_0}$	(13)	(Chittoo and Sutherland, 2019)
Thomas	$\ln\left(\frac{C_0}{C_t} - 1\right) = \frac{K_{Th}q_e m}{Q} - K_{Th}C_0 t$	(14)	(Patel, 2019)
Wol-borska	$\ln\frac{C_t}{C_0} = \frac{\beta C_0}{N_0}t - \frac{\beta Z}{U_0}$	(15)	(Patel, 2019)
Yoon-Nelson	$\ln\left(\frac{C_t}{C_0 - C_t}\right) = K_{YN}t - \tau K_{YN}$	(16)	(Patel, 2019)

K_{AB} is Adams-Bohart model constant (L mg^{-1} min^{-1}); Z is bed height (cm); N0 is volumetric sorption capacity (mg L^{-1}); U0 is solution velocity through the packed column (cm min^{-1}); KTh is Thomas model constant (mL min^{-1} mg^{-1}); m is the mass of SA-RGO beads packed in column (g); β is the kinetic coefficient of external mass transfer (mn^{-1}); qe is maximum dye uptake (mg g^{-1}); τ is the time to adsorb 50 % phenol (min) and KYN is the Yoon-Nelson rate constant (min^{-1}).

2.9. Desorption

In order to control the reuse of SA-RGO beads, desorption tests are performed. First, after a series of real effluent of OMWW treatment, the SA-RGO beads were loaded with phenolic compounds. The initial concentration was 3274.28 mg L^{-1} for a contact time of 150 min and at 25 °C. Then, the adsorbent was washed with HCl (0.5 M) for 135 min. Then, the SA-RGO beads were reused again for four cycles of adsorption. This desorption cycle was performed after each adsorption cycle.

Table 5
Physic-chemical characterization of OMWW.

Parameters (Unit)	OMWW
pH	4.6
Electrical Conductivity (mS cm^{-1})	20
COD (g-O_2 L^{-1})	101.24
Total phosphorus (mg L^{-1})	0.54
Orthophosphate (mg L^{-1})	1.69
Nitrite (mg L^{-1})	0.012
Sodium (mg L^{-1})	315
Potassium (mg L^{-1})	5810
Ammoniacal nitrogen (mg L^{-1})	0.212
Kjeldahl nitrogen (NTK) (mg L^{-1})	205
Sulfate (mg L^{-1})	2009.2
Nitrate (mg L^{-1})	0.312
Total phenol (mg L^{-1})	3274.28

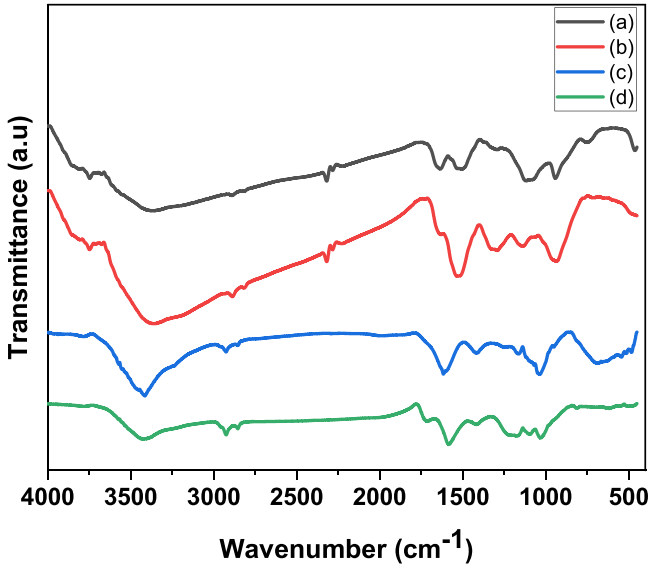

Fig. 4. FTIR spectra of GO (a), RGO (b), SA-RGO beads before (c) and after (d) and adsorption of the phenolic compounds.

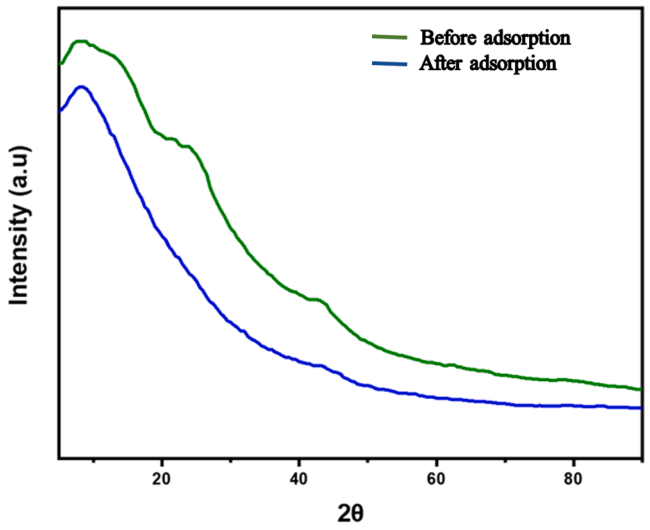

Fig. 5. XRD of SA-RGO beads before and after adsorption.

3. Results and discussion

3.1. Physic-chemical characterization of OMWW

Table 5 shows the physicochemical parameters of OMWW, and this effluent is characterized by acidic pH of 4.6 and electrical conductivity of 20 mS cm^{-1}. Similar results were obtained in previous studies (Lissaneddine et al., 2021; Bouknana et al., 2014; Dehmani et al., 2020; Haydari et al., 2022). Furthermore, the high value of the chemical oxygen demand (COD) (101,24 g O2 L^{-1}) indicates the presence of toxic compounds (Vuppala et al., 2021) and phenolic compounds (3274.28 mg L^{-1}). In addition, the characterization of OMWW showed the presence of inorganic loadings such as sodium (315 g L^{-1}) and potassium (5810 mg L^{-1}).

3.2. Characterization of the SA-RGO beads

Fig. 4 shows the FTIR spectra of GO (a), RGO (b) and SA-RGO before (c) and after (d) adsorption. In the GO spectrum, the peaks are the stretching of the hydroxyl function -OH (3380 cm^{-1}), epoxide group C-O (1100 cm^{-1}), C≡C stretching (2320 cm^{-1}), C═C vibrations (1520 cm^{-1}, and C═O stretching of carbonyl (1640 cm^{-1}) (Moon et al., 2010). The exitance of these oxygen-containing functions validated the oxidation of graphite to GO. In addition, the disappearance of carbonyl and hydroxyl functions in the FTIR spectra of the RGO, approving the reduction of GO to RGO. The RGO spectrum shows the presence of other bands such as C-O epoxide stretching (1150 cm^{-1}), C═C stretching (1520 cm^{-1}) and C≡C stretching (2310 cm^{-1}). FTIR spectra of SA-RGO (Fig. 4c), the peak at 3410 cm^{-1} is awarded to oxygen and hydrogen stretching. Other bands were observed around 2920 cm-1, which can be generated through aliphatic C-H vibrations. The peak at 2850 cm^{-1} is attributed to -O-CH_3 or two bands for the aldehyde group R−CH═O (Ahmad et al., 2007). The bands at 1020 and 1610 cm^{-1} can be due to the alcoholic groups and C═C stretching for unsaturated aliphatic forms (Bandosz and Block, 2006). After the adsorption process (Fig. 4d), a peak was observed at 3408 cm^{-1}; it is attributed to OH stretching vibrations (carboxylic acids, alcohols and phenols). The peak at 1590 cm^{-1} can be assigned to amine and/or carboxylate, and the peak at 1300 cm^{-1} corresponds to C-H of CH_3 groups or COO antisymmetric stretching. The band at 1020 cm^{-1} is due to carbohydrates of polysaccharides. The bands at 1710 cm^{-1} can be assigned to the symmetric COO stretching bands of the alginate molecule (Ahmad et al., 2007).

The XRD pattern of SA-RGO before and after phenol adsorption is shown in Fig. 5. These diffractograms indicate a typical amorphous nature, suggesting that the phenol molecules diffuse into the micropores and macropores of SA-RGO. A significant difference was observed in the intensity of peaks in the XRD spectrum before and after phenol adsorption. The intensity of the diffraction peaks decreased in SA-RGO adsorbed by phenol. The result suggests that phenol-adsorbed SA-RGO may not induce bulk phase changes (Arulkumar et al., 2011). The decrease in peak intensity after adsorption also indicates that the phenol molecules began to fill the pores as the adsorption progressed (He et al., 2022).

SEM images of the RGO and SA-RGO beads are shown in Figs. 6a and 6b. Alginate and $CaCl_2$ can establish a rigid structure on the alginate that generates hollow ions to calcium to join, each ion of which can bind to four units. The design represents the ionotropic gelation of alginate and is named the "egg box" model (Aziz et al., 2020).

Fig. 6a shows a less homogeneous and porous surface than the surface of the SA-RGO beads, exhibiting a distorted and intertwined

Table 6
EDS of GO, RGO and SA-RGO beads.

Element	GO	RGO	SA-RGO beads
	Atomic %	Atomic %	Atomic %
C	51.15	73.56	16.59
N	3.94	0.02	00.00
O	43.59	21.16	45.47
Ca	00.00	00.00	34.00
Na	00.00	0.56	2.26
S	1.32	2.63	00.00
Cl	00.00	2.07	1.69
Totals	100	100	100

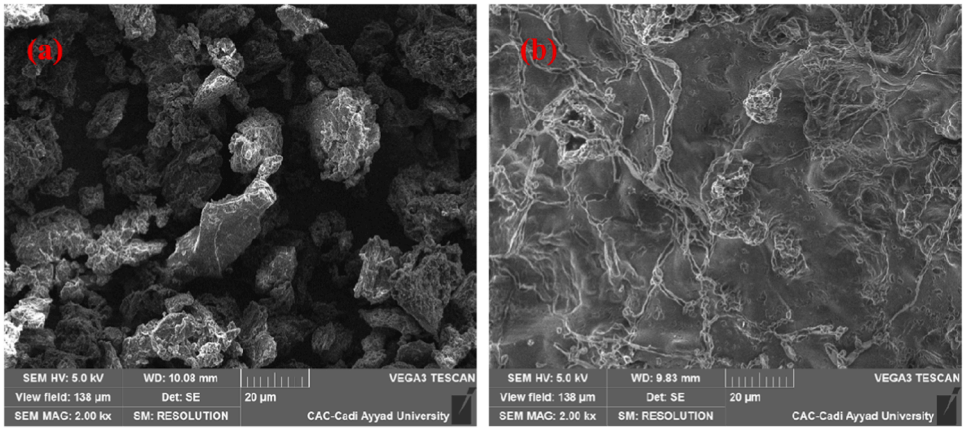

Fig. 6. SEM of RGO (a) and SA-RGO beads (b).

Table 7
Textural characteristics of SA-RGO beads.

Parameters	S_{BET} (m^2 g^{-1})	Total pore volume (cm^3 g^{-1})	r^- (nm)
Value	1030	1.09	2.11

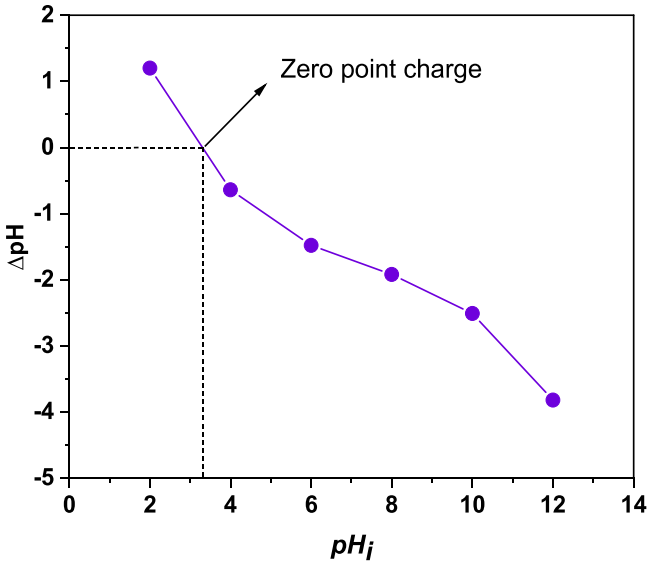

Fig. 7. Point of zero charges of SA-RGO beads.

structure (Fig. 6b). This structure is useful because it improves the mechanical strength of the SA-RGO beads and promotes high porosity (Yuney et al., 2020). In addition, RGO encapsulation increases the specific surface area of the SA-RGO beads and the active adsorption site, which is crucial to promote the adsorption capacity of phenol. Therefore, the porous surface organization should be considered an agent for expanding the surface area and permeability of the composite beads. In addition, these cavities facilitate pore diffusion upon adsorption due to the large internal specific surface area with low diffusion resistance in the composite beads (implying advanced adsorption potential and rate). This micrograph's porous nature is evident (Aziz et al., 2020).

To determine the % yield of GO using *Verbena officinalis*, based on the EDS results presented in Table 6. The O:C ratio of GO synthesized by the modified hummer's method was 0.85. In addition, the O:C ratio of prepared SA-RGO beads was 0.28. These results indicate the successful application of *Verbena officinalis* extracts as a reducing agent for removing oxygen functional groups. However, this ratio is always variable for other green RGO synthesis work depending on the synthesis process and the original GO state (Rout and Jena, 2022).

The textural characteristics of the SA-RGO beads are presented in Table 7. The specific surface area (SBET) of beads was 1030 m^2 g^{-1}. In addition, the total pore volume (VT) value was 1.09 cm^3 g^{-1}. Yuney et al. (2020) activated the olive cake by CuO and reported SBET and VT values of 536.55 m^2 g^{-1} and 0.0678 cm^3 g^{-1}, respectively. The average value of r^- was 2.11 nm. These results show the higher adsorption capacities of SA-RGO beads. The application of resource-saving technologies, such as adsorption using locally available materials and resource recovery to obtain value-added products (e.g., phenol), will not only facilitate the removal of harmful contaminants from water or wastewater but will also be cost-effective on an industrial scale (Aziz et al., 2020).

Fig. 7 shows that the pHzpc (point of zero charges) of SA-RGO beads is 3.2. At pH values above 3.2, the charge of SA-RGO beads is negative; at pH values above 9.89, the dominant charge of phenol is negative. The negative charge of SA-RGO beads and phenol at basic pH is the reason behind the appearance of the electrostatic repulsion forces between them, implying weak adsorption. In addition, there is no electrostatic repulsion force at acidic pH, which increases the adsorption efficiency. Therefore, it seems that at basic pHs, the phenol ions compete to occupy the surface of SA-RGO beads, which may decrease adsorption efficiency (Li et al., 2009).

3.3. Reduction mechanism: phytochemistry

The chromatographic profile (Fig. 8) shows the presence of major phenolic compounds that may be involved in the green synthesis of GO. Mass (m)/charge ratios (z) and retention times were applied to determine five bio-compounds. Table 8 presents the identified phytochemical compounds found in *Verbeinea officinalis* studied. They are: Verbenalin (RT = 5.06 min), Apigenin-7-O-glucoside (RT = 15.32 min), Apigenin 7-O-diglucuronide (RT = 18.38 min), Verbascoside (RT = 21.8 min) and Apigenin (RT = 26.18 min). The other detected phytochemicals belong to the flavonoids. All these organic molecules play a veritable role in GO reduction (Mahmoud et al., 2022). Flavonoids are more often recognized as important contributors to the reducing ability of *Verbena*

Table 8
Identified phytochemical compounds found in *Verbeinea officinalis* by UHPLC.

No	RT	Λ_{max} (nm)	*m/z* (M-H)-	Proposed compound	Molecular formula
1	5.06	-	387.1	Verbenalin	$C_{17}H_{24}O_{10}$
2	15.32	266.336	431.1	Apigenin-7-O-glucoside	$C_{21}H_{20}O_{10}$
3	18.38	267.336	621.4	Apigenin 7-O-diglucuronide	$C_{27}H_{26}O_{17}$
4	21.8	280	622.1	Verbascoside	$C_{29}H_{35}O_{15}$
5	26.18	266.336	269.1	Apigenin	$C_5H_{10}O_5$

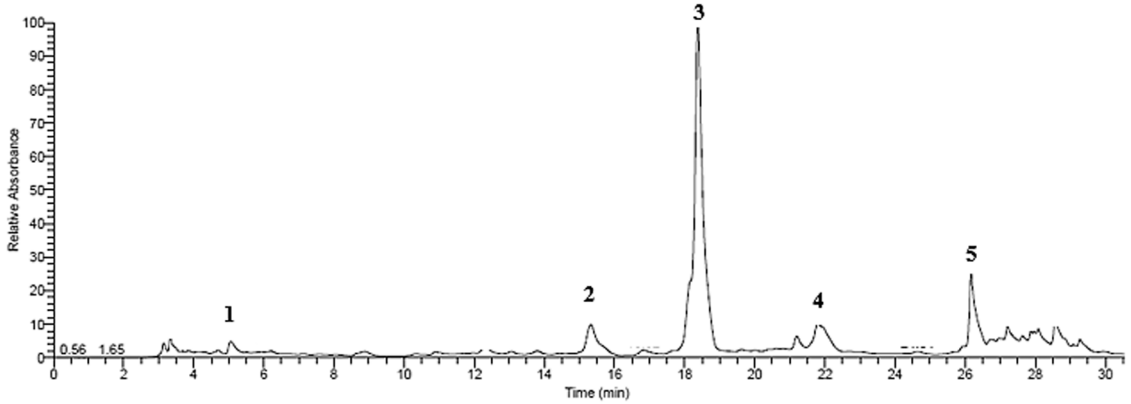

Fig. 8. Profile chromatographic of *Verbeinea officinalis* powder at 280 nm.

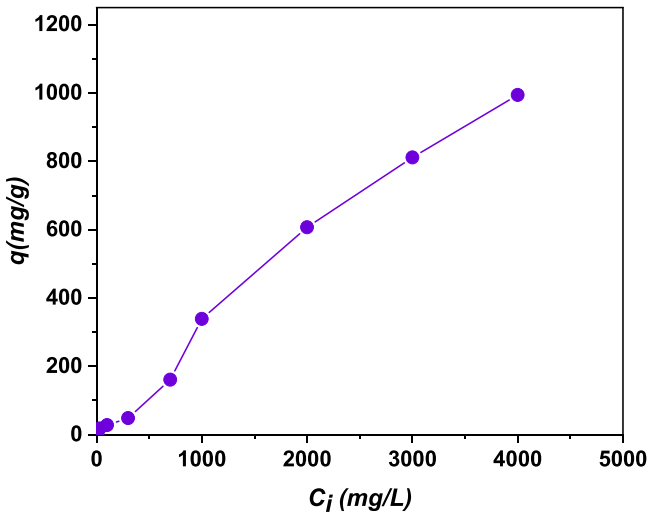

Fig. 9. Initial concentration effect.

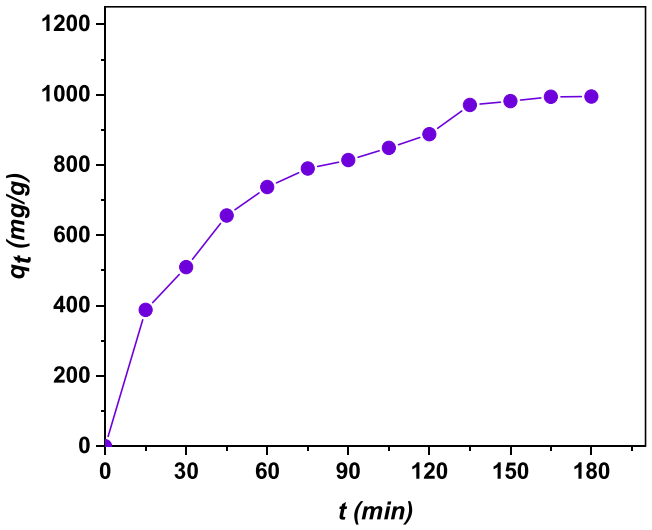

Fig. 10. Contact time effect.

officinalis (Bhattacharya et al., 2017).

3.4. Adsorption results

3.4.1. Batch adsorption

3.4.1.1. Effect of initial concentration. Initial concentration is one of the most important factors affecting the adsorption process. The driving force provided by the initial concentration of phenol allows controlling the mass transfer resistances between the liquid and the solid phase (Lin and Juang, 2009). A series of concentrations: 10, 30, 100, 300, 700, 1000, 2000, 3000 and 4000 mg L^{-1}, were performed for 180 min

The performance of the SA-RGO beads in the function of the phenol's initial concentration is presented in Fig. 9. The figure shows an increase in adsorption capacity from 4.85 to 994.75 mg g^{-1} with an increase in initial concentration from 10 to 4000 mg L^{-1}. A similar increasing trend is noted for phenol adsorption, which is consistent with the results of Yuney et al. (2020), and Ververi and Goula (2019). This increase in adsorption capacity can be likened to a higher driving force to control the transfer resistance of phenol between the solid and liquid phases, causing a higher possibility of adsorbent-adsorbent collision (Ververi and Goula, 2019). As an explanation, Mohd Din et al. (2009) suggested

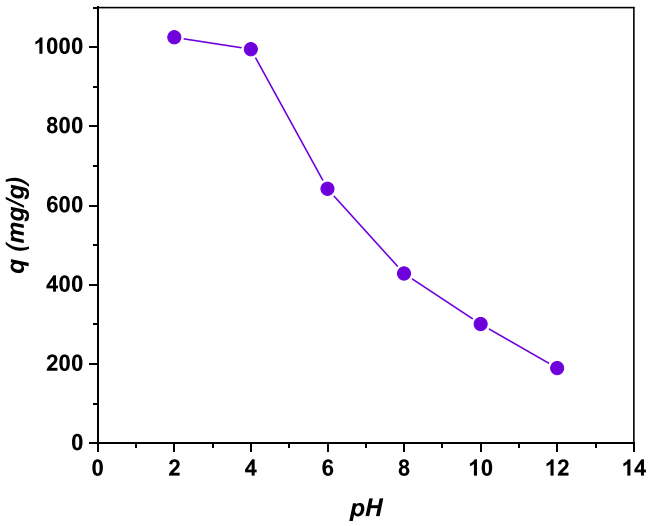

Fig. 11. Effect pH.

that when the adsorbent surface was nearly saturated with adsorbate, the second phenomenon of intra-particle diffusion would be initiated, slowly increasing the adsorbate adsorption operation.

3.4.1.2. Effect of contact time. Fig. 10 presents the effect of contact time on the adsorption mechanism of phenolic compounds in SA-RGO beads. The equilibrium adsorption time was 135 min. At this stage, the adsorbate concentration is stabilized in the solution and does not cause any change. However, the adsorption rate before the equilibrium time is fast due to the many adsorption sites available on the surface of SA-RGO beads. In addition, the amount of phenolic compounds accumulated on the SA-RGO bead's surface increases rapidly. Then, the remaining sites are difficult to occupy as repulsive forces increase between the adsorbate bound to the bulk phase and the solid surface. Moreover, phenolic compounds are small molecules that can be penetrated the internal pores, which decreases the driving force of mass transfer between the liquid and solid phases over the contact time (Allen et al., 2005). Obviously, after 135 min, the phenolic molecules encounter great resistance to diffuse into the internal pores, so this step is slower (Allen et al., 2005; Achak et al., 2009). Therefore, the equilibrium time varied depending on the adsorbate and the nature of the adsorbent's surface studied and according to the adsorption study. The equilibration time of phenolic compounds on SA-RGO beads was faster (120 min) than other adsorbents studied, such as banana peel (3 h) (Achak et al., 2009), activated carbon (4 h) (Azzam et al., 2004), wheat husk (5 h) (Jagwani and Joshi, 2014), coconut shell (5 h) (Mohd Din et al., 2009), and wheat bran (4 h) (Achak et al., 2014). In contrast, Ververi and Goula (2019), who studied the adsorption of phenol on the by-products of pomegranate peel and orange juice, found an equilibrium time of 20 min

3.4.1.3. Effect of pH. The pH is a significant factor in the adsorption mechanism. Alteration of the solution pH leads to changes in the external surface characteristics of the adsorbents, which influences the electrostatic interaction between the phenol molecules and the surface of SA-RGO beads. In addition, the hydrogen ion dissociation of phenolic compounds strongly depends on the pH (Achak et al., 2009). Therefore, to determine the pH effect on the adsorption mechanism, several tests were conducted in a pH range from 2.0 to 12.0 while keeping the other adsorption factors constant, such as initial concentration (4000 mg L^{-1}), temperature (25 °C) and contact time (180 min).

Fig. 11 displays that the adsorption capacity of phenolic compounds decreased with increasing pH; it decreased from 1024.84 to 189.73 mg g^{-1} when the pH increased from 2 to 12. The pH of the solution exceeds 4.0, and the adsorption capacity of phenol decreases

Table 9
Equilibrium parameters for phenolic compounds adsorption.

Model	Parameters	Value
Langmuir	qm (mg g^{-1})	588
	K_L (L/mg)	0.0021
	R^2	0.570
Freundlich	K_F ($mg^{1-(1/n)}$ $L^{1/n}$ g^{-1})	3.94
	n	1.50
	R^2	0.999

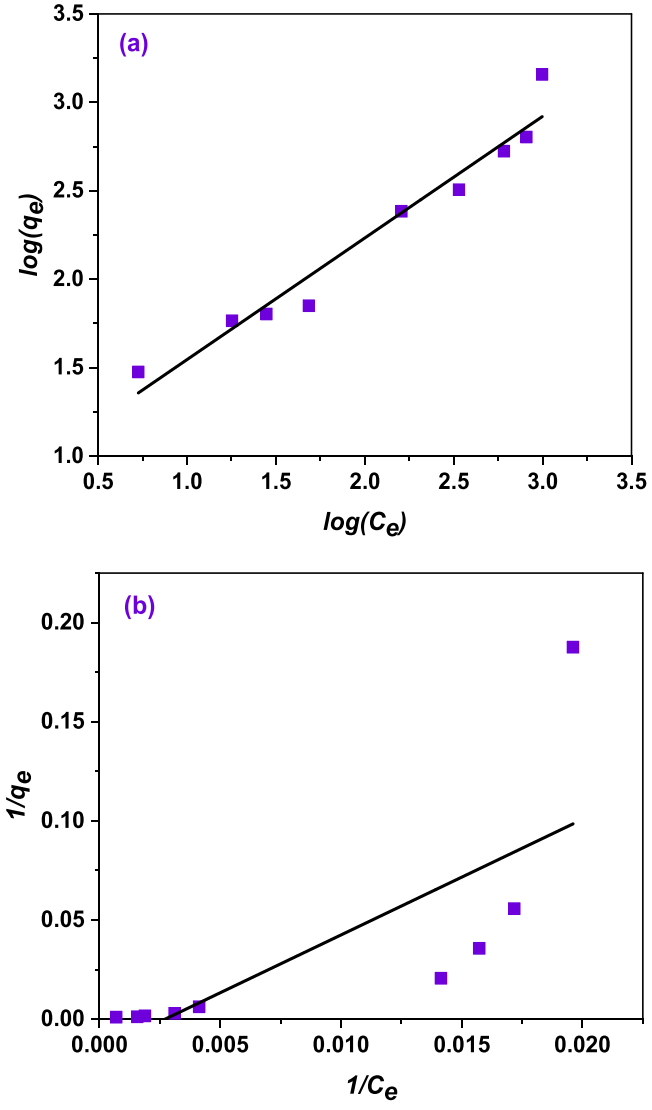

Fig. 12. Modeling the sorption isotherm of phenolic compounds by Freundlich (a) and Langmuir (b).

sharply because, at basic pH, the repulsive force between the surface of SA-RGO beads and phenolic ions is higher, resulting in low removal. In addition, the solubility of phenol increases with decreasing pH values (Lissaneddine et al., 2021). As the phenol's pKa is 9.8, its protonated form is predominant between acid and neutral pH. The protonated form is preferable to be adsorbed on the surface of SA-RGO beads than the non-protonated form. These reasons explain the increase in adsorption capacity when the pH decreases. Similar results were obtained by Thaworchaisit and Pakulanon (2007), Sun et al. (2019), and Al Bsoul et al. (2020), and Tahermansouri et al. (2015). They reported that the highest adsorption capacity is obtained in acidic media.

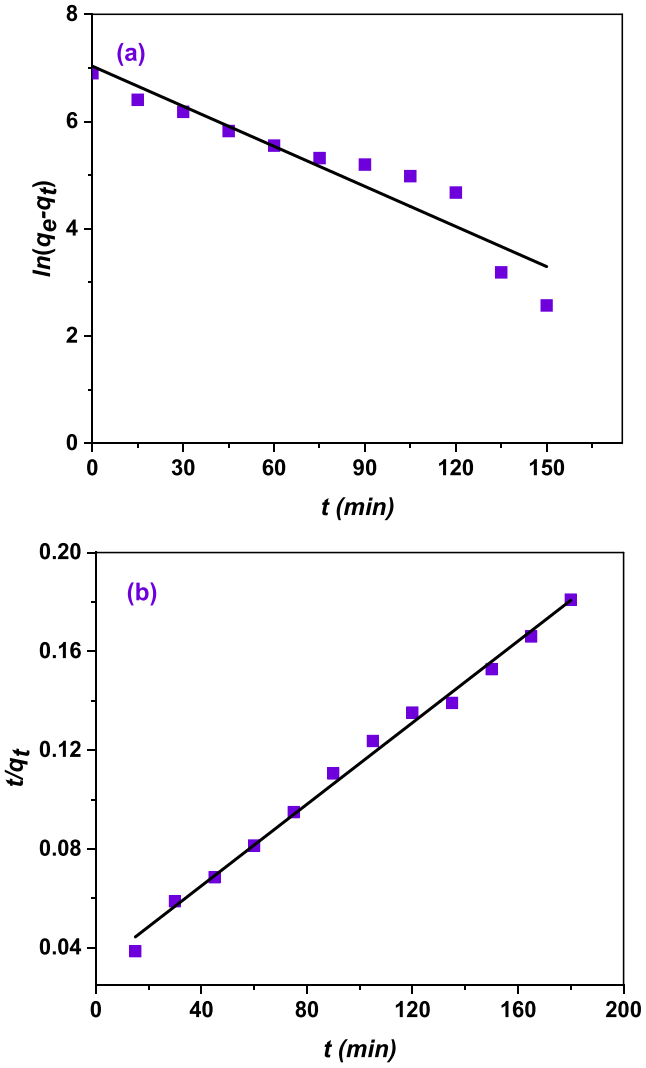

Fig. 13. Kinetic models: pseudo-first-order (a) and pseudo-second-order (b) kinetics models.

Table 10
Kinetic factors for the adsorption process of phenolic compounds.

q_e (exp) (mg g^{-1})	Pseudo-first-order			Pseudo-second-order		
	q_e(cal)	K_1	R^2	q_e(cal)	K_2	R^2
994.759	1654.57	0.035	0.89	1111.1	3.4710^{-5}	0.994

3.4.1. 4. Adsorption isotherms. Table 9 shows the parameters of the three isothermal models used in this work. The correlation coefficient R^2 of the Freundlich model is high. This indicates that this model better describes the adsorption of phenol on SA-RGO beads compared to the other Langmuir model.

The Freundlich model is based on assumptions, such as adsorption is assumed to be reversible, occurs on both homogeneous and heterogeneous surfaces and by both physical and chemical adsorption (Liu et al., 2019). All adsorption sites are energetically identical, with a non-uniform heat distribution on the adsorbent surface; adsorption energy is distributed according to an exponential law as a function of the heat of adsorption. The parameters n and K_F indicate the adsorption intensity and the adsorption capacity on SA-RGO beads, respectively; in this study $K_f = 3.94$ and $n = 1.50$. A higher value for 1/n shows that removing phenol with SA-RGO beads is favorable. Several types of research on the adsorption of phenolic compounds from OMWW have

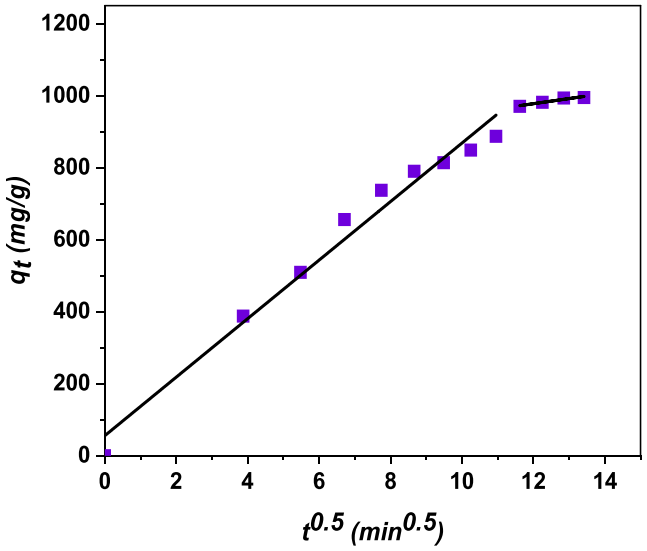

Fig. 14. Intra-particle diffusion kinetic model.

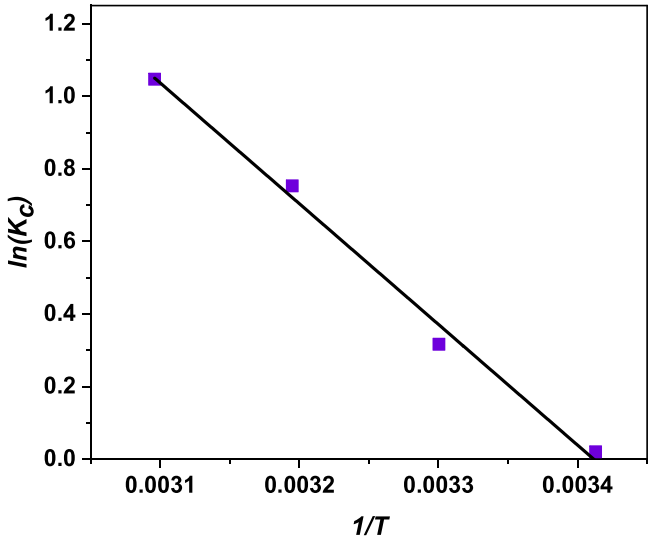

Fig. 15. ln(Kc) as function of 1/T.

Table 11
Intra-particle diffusion parameters.

First step ($0 \leq t^{0.5}$ ($min^{0.5}$) ≤ 10.95)			Second step ($10.95 < t^{0.5}$ ($min^{0.5}$) ≤ 13.41)		
K_{id1}	C_1	R_2	K_{id2}	C_2	R^2
81.307	55.067	0.976	14.25	806.6	0.925

Table 12
Thermodynamic parameters.

ΔG^0 (kJ mol^{-1})				ΔH^0 (kJ mol^{-1})	ΔS^0 (kJ mol^{-1} K^{-1})
293	303	313	323		
- 0.915	- 1.46	- 2.85	- 9.71	35.22	0.1193

found that the Freundlich model is the model that gives a better explanation of the adsorption prowess of phenol (Bertin et al., 2011; Ena et al., 2012; Chkili and Abderrabba, 2015; Achak et al., 2009; Ververi and Goula, 2019; and Vavouraki et al., 2020). Several similar studies on the removal of phenol show a low adsorption capacity, namely Lissaneddine et al. (2021) (68 mg g^{-1}), Allaoui et al. (2020) (161 mg g^{-1}), Göktepeli et al. (2021) (7.06 mg g^{-1}), Aly et al. (2018) (16.5 mg g^{-1}), Njimou et al. (2021) (92.75 mg g^{-1}), Elayadi et al. (2020) (57.5 mg g^{-1}) and Aliakbarian et al. (2015) (156.2 mg g^{-1}). However, this study shows a very high value of adsorption capacity (994 mg g^{-1}) (Fig. 12).

3.4.1.5. Kinetic studies. The curves and kinetic parameters linked to the two pseudo-first-order and pseudo-second-order kinetic models are present in Fig. 13 and Table 10, while the corresponding fitted plot and parameters related to the intra-particle diffusion model are described in Fig. 14 and Table 11. Table 10 shows the regression results certified that the pseudo-second-order model with the highest correlation coefficient R^2 (0.994) provides better results than the pseudo-first-order model for interpreting the kinetic adsorption data of phenolic compounds. Moreover, the equilibrium adsorption capacity of phenolic compounds calculated in the pseudo-second-order kinetic model q_e = 1111.1 mg g^{-1} is closer to the value of the experimental adsorption capacity q_e = 994.759 mg g^{-1} compared to that obtained from the pseudo-first-order model q_e = 1654.57 mg g^{-1}. According to Achak et al. (2009), this result shows that chemisorption plays a role in the adsorption mechanism, which may be partly due to the hydrogen bonding between the active functional groups in the adsorbents and the hydroxyl groups of the phenolic compounds, and which may be the rate-limiting step. While the first and second-order kinetic equations cannot give an idea about the internal diffusion mechanism, the application of the intra-particle diffusion kinetic model would be advantageous in studying the transfer of adsorbed particles from the adsorbent solid surface to the internal pores (Abdi et al., 2017). If the plot of q_t vs. $t^{0.5}$ is a straight line that passes through the origin, the adsorption rate would be checked by intra-particle diffusion throughout the adsorption period. However, if the evolution shows more than one linear zone and the slope of the first zone is not zero, diffusion initially controls the adsorption rate (Hameed and Rahman, 2008). The other lines correspond to the successive stages of mass transfer with decreasing velocities: intra-particle diffusion in the adsorbent's macro, meso and micropores (Hameed and Rahman, 2008). Fig. 14 shows that the adsorption of phenolic compounds is composed of two linear zones, notable adsorption on the surface of SA-RGO beads and intra-particle diffusion.

In addition, according to Table 11, the significant difference between the rate constant of the first K_{id1} = 81.307 is greater than the second K_{id2} = 14.25, indicating that the greater amount of adsorption occurs initially by adsorption of phenolic compounds on the surface of SA-RGO beads due to the availability of active sorption sites (Anisi et al., 2021). Then, intra-particle diffusion of adsorbate particles to the sites of the inner surface of SA-RGO beads begins. This stage is considered the rate-limiting step of adsorption. Although the constants C_1 and C_2 of the intra-particle diffusion obtained approach zero (Table 11), which shows that the adsorption rate is not only evaluated by the intra-particle diffusion. As a result, the rate and speed of adsorption are estimated by film diffusion and intra-particle diffusion (Gundogdu et al., 2012).

3.4.1.6. Thermodynamic analysis. To better understand the nature, spontaneity, and feasibility of the adsorption of phenolic compounds, thermodynamic parameters were determined, including standard enthalpy change ΔH° (kJ mol^{-1}), standard Gibbs free energy change ΔG° (kJ mol^{-1}), and standard entropy change ΔS° (kJ mol^{-1} K^{-1}).

Fig. 15 shows the linear plot of ln(Kc) versus 1/T, the values of ΔS° and ΔH° are determined from the slope and intercept of the curve. The results of Gibbs free energy change ΔG° in the adsorption of phenolic compounds on SA-RGO beads were determined as a negative value for all temperature values examined. For this cause, it can be deduced that the adsorption of phenolic compounds is applicable and spontaneous (Table 12). In general, ΔG° change lies in the range of 0 to - 20 kJ mol^{-1} for physisorption, - 20 to 80 kJ mol^{-1} for the existence of chemisorption and physisorption, and - 80 to - 400 kJ mol^{-1} for chemisorption

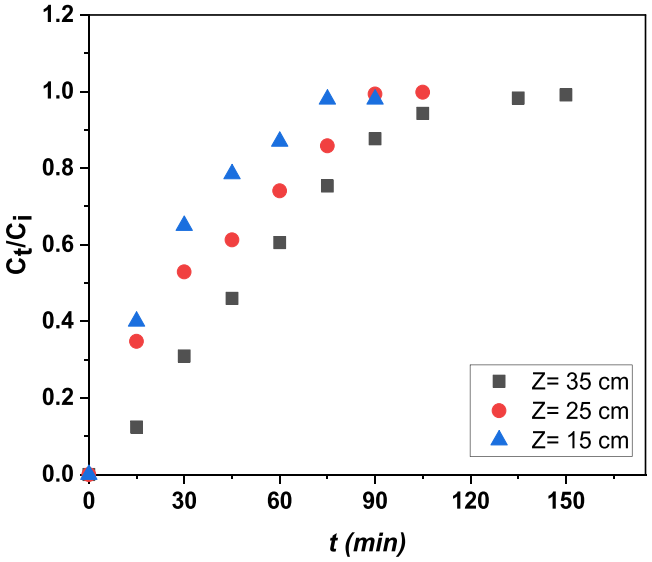

Fig. 16. Influence of packing height on breakthrough curves for sorption of phenolic compounds (pH = 4.0, C_i = 3274.28 mg L^{-1}, Q = 0.5 mL min^{-1}).

Table 13
Adsorption results using fixed-bed column.

C_i (mg L^{-1})	V_{ef} (mL)	Q (mL min^{-1})	m_{total} (g)	q_e (mg g^{-1})	R (%)
3274.28	67.5	0.5	5	967	87

(Anirudhan and Radhakrishnan, 2010). The ΔG° values confirm that the adsorption mechanism is dominated by physisorption. A positive sign in the enthalpy change ΔH° indicates that the mechanism is endothermic. The result ΔS° indicates that the randomness is increased at the solution/solid (Gupta et al., 2017).

3.5. Fixed-bed column

Adsorption of phenolic compounds via fixed-bed column was proposed as an alternative method (Lissaneddine et al., 2021; Benaddi et al., 2022). The SA-RGO beads were applied as adsorbents.

The analysis of the influence of different column heights (Z = 15, 25 and 35 cm) with a flow rate (Q = 0.5 mL min^{-1}) on the breakthrough profiles was represented in Fig. 15. The percentage removal of phenolic compounds increased significantly from 60 % to 87 % with increasing height from 15 to 35 cm, respectively. The increase in percent removal is due to the column's elongation of the mass transfer zone. Therefore, the greater mass of SA-RGO beads available, the higher the packing height, which leads to an augment in adsorption sites, thus, the longer time for bed exhaustion (Azzaz et al., 2017).

The study of the influence of the effluent flow rate (Q = 0.5, 1 and 2 mL min^{-1}) on the breakthrough profiles was represented in Fig. 16. Increasing the flow rate minimizes percent removal, which was assigned to the shortening of the residence time of the phenolic compound in the packed bed, which prevents their proper diffusion into the SA-RGO beads sites (Khadhri et al., 2019). As a result, the removal rate decreased from 87 % (0.5 mL min^{-1}) to 50 % mg g^{-1} (3 mL min^{-1}). A similar result was previously studied for phenol adsorption using activated Corn Cobs (Rocha, 2015).

The results showed better results for a flow rate of 0.5 mL min^{-1} and a height of 40 cm. Fig. 16 shows a plot of C_t/C_0 versus time (Q = 0.5 mL min^{-1}; Z = 40 cm). All phenol was adsorbed for the first 30 min, which decreased the phenol concentration. During adsorption, the concentration of phenolic compounds at the outlet gradually increases until Ct = Ci and the curve becomes almost flat. This increase is

Table 14
Adams-Bohart, Thomas, Yoon-Nelson and Wol-borska model parameters.

Model	Parameters	Value
Adams-Bohart	K_{AB}	0.000066
	N_0	2103.80
	R^2	0.7478
	RMSE	0.1263
Thomas	K_{Th}	0.000197
	q_{Th}	1074.51
	R^2	0.97
	RMSE	0.0119
Wol-borska	N_0	2102
	β	0.14
	R^2	0.7478
	RMSE	0.1261
Yoon-Nelson	K_{YN}	0.216
	τ	45.03
	R^2	0.97
	RMSE	0.0119

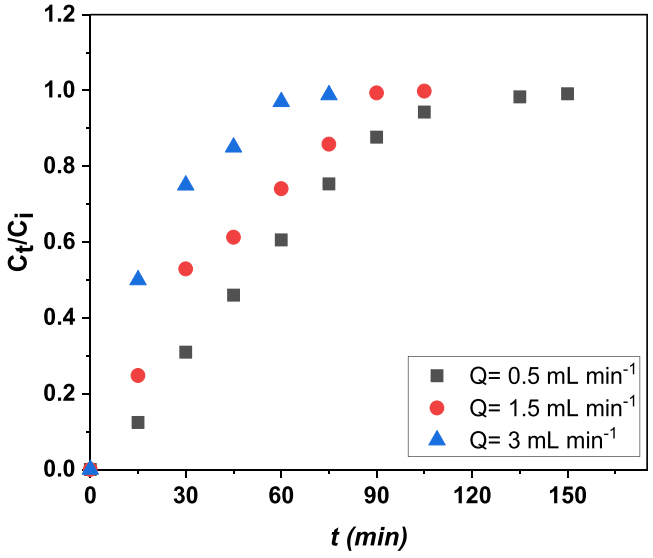

Fig. 17. Influence of flow rate on breakthrough curves for sorption of phenolic compounds (pH = 4, Z = 35 cm, C_i = 3274.28 mg L^{-1}).

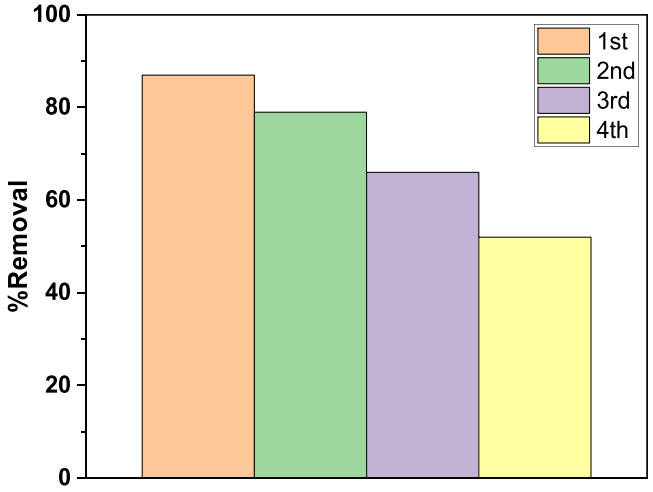

Fig. 18. Removal of phenolic compounds using SA-RGO beads in four consecutive desorption cycles using HCl as eluent.

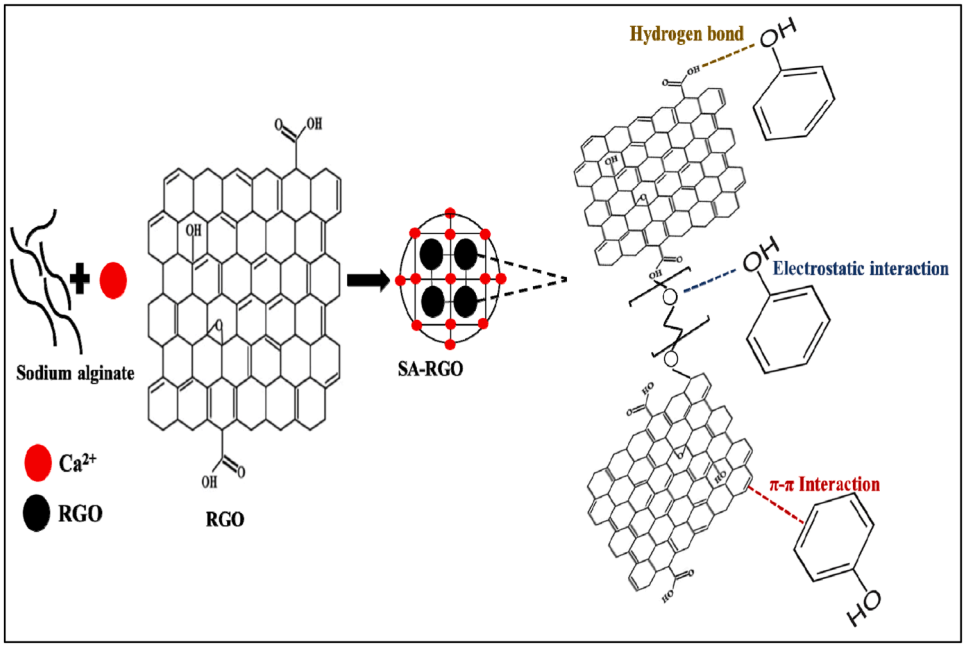

Fig. 19. Schematic diagram for proposed phenol removal mechanism.

due to the saturation of the pores of the SA-RGO beads (Kundu and Gupta, 2005). The present study, the q_e value attained 967 mg g^{-1} for Q = 0.5 mL min^{-1} and C_i = 3274.28 mg L^{-1}, with an elimination rate of 87 % (Table 12).

The applied model parameters obtained according to the linear regression are presented in Table 13. The R^2 of the Yoon-Nelson and Thomas models are equal (0.97) and close to unity compared to the R^2 values of the Adam Bohart and Wolborska models (0.7478). The value of the parameter q_{Th} = 1074.51 mg g^{-1} estimated using the Thomas model is close to the value of the experimental capacity q_e = 967 mg g^{-1}. The error value calculated using the Thomas and Yoon Nelson equation is also very small (0.0119) compared to the Adam-Bohart and Wolborska equation (0.1263). In conclusion, the Yoon-Nelson and Thomas models presented the experimental results well (Table 14).

3.6. Desorption

Reusing a sorbent is an aspect from the economic point of view because it allows prolonged use of adsorbent; the possibility of reusing material is related to its regeneration capacity. The desorption step of SA-RGO beads was performed at 25 °C for 135 min; afterward, the sorbent was regenerated using a diluted acid solution and then reused to remove phenolic compounds to check its sorption capacity at the equilibrium state. Fig. 17 shows the equilibrium sorption capacity of phenol for four cycles of SA-RGO bead use. In the first two adsorption cycles, the removal rate decreased from 87 % to 79 %. Subsequent cycles showed a more significant decrease in elimination rate, with a reduction of about 35 % for the fourth use compared to the first adsorption cycle.

The adsorption efficiency was 87 %, indicating that the sorption mechanism for removing phenolic compounds is an effective method for the treatment of OMWW compared to other adsorbents that have been previously used to treat OMWW (Adhoum and Monser, 2004; Paraskeva et al., 2007; El-Abbassi et al., 2014) (Fig. 18).

3.7. Adsorption mechanism

Several studies have reported various mechanisms for removing phenolic compounds through adsorption. Among these, the three most widely accepted mechanisms are (a) π-π electron pairing interaction, (b) electron donor-acceptor interaction (electrostatic interaction), and (c) hydrogen bonding interactions. The presence of oxygen functional groups of SA-RGO at the π-electron-rich regions provides complexes with aromatic rings of phenol pollutants. During adsorption, the π-electron rich regions of SA-RGO act as a donor, and the phenol rings as acceptors. Therefore, the adsorption of phenol onto SA-RGO is controlled by the dispersive interaction of π-π electrons (Rout et al., 2022). During the adsorption of phenol, two different electron donor-acceptor interactions occur. The first involves the interaction of the hydroxyl and carbonyl groups (electron donor) of SA-RGO with the aromatic ring of the phenol pollutant (electron acceptor). The interaction between the donor and acceptor of SA-RGO and phenol during the adsorption mechanism depends on the dipole moment of the different functional groups present on the basal plane (Mojoudi et al., 2019). Adsorption on the SA-RGO surface is due to the formation of hydrogen bonds between the hydrogen and oxygen of the adsorbent and the phenol molecule (Dąbrowski et al., 2005). In addition, a host-guest inclusion complex is formed between SA-RGO and phenol through Van der Waals forces and hydrogen bonding. Therefore, more and more phenol molecules are attracted to the surface of the adsorbent, which enhances the adsorption process. Since the reaction between the phenol molecule and the SA-RGO occurs over the entire surface of the SA-RGO, the adsorbed phenol molecules are uniformly distributed on the SA-RGO. The schematic presentation of the adsorption mechanism of phenol on SA-RGO is shown in Fig. 19.

4. Conclusion

The green reduction of graphene oxide was made by *Verbena officinalis*, targeting a green chemistry application. FTIR, SEM, and EDS characterized the prepared SA-RGO beads. Batch and column adsorption test to define the ideal conditions for sorption of phenolic compounds from OMWW. The Freundlich models and pseudo-second-order best represented the sorption isotherm and kinetics. The optimized adsorption parameters were 3.68 g L^{-1} of adsorbent dosage, pH of 4.0, adsorption time of 135 min, and temperature of 25 °C. The reaction was endothermic and applicable. The Yoon-Nelson and Thomas model best predicts the column adsorption of phenolic compounds. However, the adsorption efficiency decreases from 87 % to 52 % after four adsorption

cycles. This work gives a new green approach to synthesizing RGO to prepare composite beads (SA-RGO beads), which can be applied as a suitable adsorbent to eliminate the phenol from OMWW. However, sodium alginate's mechanical strength and stability are relatively low. Furthermore, ion exchange on the cross-linked calcium ions could lead to the decomposition of the synthesized materials, which limits the regeneration of the adsorbent, indicating a future research prospect.

Declaration of Competing Interest

The authors declare that they have no known competing financial interests or personal relationships that could have appeared to influence the work reported in this paper.

Acknowledgments

This research was financed by the Morocco-Tunisian Bilateral Scientific Cooperation Project (20/PRD-MT-02).

References

Abdi, J., Vossoughi, M., Mahmoodi, N.M., Alemzadeh, I., 2017. Synthesis of amine-modified zeolitic imidazolate framework-8, ultrasound-assisted dye removal and modeling. Ultrason. Sonochem. https://doi.org/10.1016/j.ultsonch.2017.04.030.

Achak, M., Hafidi, A., Mandi, L., Ouazzani, N., 2014. Removal of phenolic compounds from olive mill wastewater by adsorption onto wheat bran. Desalin. Water Treat. https://doi.org/10.1080/19443994.2013.819166.

Achak, M., Hafidi, A., Ouazzani, N., Sayadi, S., Mandi, L., 2009. Low cost biosorbent "banana peel" for the removal of phenolic compounds from olive mill wastewater: kinetic and equilibrium studies. J. Hazard. Mater. doi: 10.1016/j.jhazmat.2008.11.036.

Adhoum, N., Monser, L., 2004. Decolourization and removal of phenolic compounds from olive mill wastewater by electrocoagulation. http://www.doi.org//10.1016/j.cep.2003.12.001.

Ahmad, A.L., Loh, M.M., Aziz, J.A., 2007. Preparation and characterization of activated carbon from oil palm wood and its evaluation on Methylene blue adsorption. Dyes Pigments. https://doi.org/10.1016/j.dyepig.2006.05.034.

Al Bsoul, A., Hailat, M., Abdelhay, A., Tawalbeh, M., Al-Othman, A., Al-kharabshehIsra, N., Al-Taani, A.A., 2020. Efficient removal of phenol compounds from water environment using ziziphus leaves adsorbent. Sci. Total Environ. https://doi.org/10.1016/j.scitotenv.2020.143229.

Aliakbarian, B., Casazza, A.A., Perego, P., 2015. Kinetic and isotherm modelling of the adsorption of phenolic compounds from olive mill wastewater onto activated carbon. Food Technol. Biotechnol. https://doi.org/10.17113/ftb.53.02.15.3790.

Allaoui, S., Naciri Bennani, M., Ziyat, H., Qabaqous, O., Tijani, N., Ittobane, N., 2020. Kinetic Study of the Adsorption of Polyphenols from Olive Mill Wastewater onto Natural Clay. Ghassoul. Journal of Chemistry. http://.org//doi:10.1155/2020/7293189.

Allen, S.J., Gan, Q., Matthews, R., Johnson, P.A., 2005. Kinetic modeling of the adsorption of basic dyes by kudzu. J. Colloid Interface Sci. https://doi.org/10.1016/j.jcis.2004.12.043.

Aly, A.A., Alashgar, K.N.S., Al-Farraj, A.S., Ibrahim, H.M., 2018. Contaminants and salinity removal of olive mill wastewater using zeolite nanoparticles. Sep. Sci. Technol. https://doi.org/10.1080/01496395.2018.1425301.

Anirudhan, T.S., Radhakrishnan P.G., 2010. Adsorptive performance ofan amine-functionalized poly (hydroxyethylmethacrylate)-grafted tamarind fruit shell for vanadium (V) removal from aqueous solutions. Chem. Eng. J. ⟨https://jglobal.jst.go.jp/en/detail?JGLOBAL_ID=201002269535402258⟩.

Anisi, M., Ghoreyshi, A.A., Mehrvarz, E., Rahimpour, A., 2021. Synthesize optimization, characterization, and application of ZIF-8 adsorbent for elimination of olive oil from aqueous solution. Environ. Sci. Pollut. Res. https://doi.org/10.1007/s11356-020-11283-0.

Arulkumar, M., Sathishkumar, P., Palvannan, T., 2011. Optimization of Orange G dye adsorption by activated carbon of Thespesia populnea pods using response surface methodology. ⟨https://doi.org/10.1016/j.jhazmat.2010.11.067⟩.

Atallah, E., Kwapinski, W., Ahmad, M.N., Leahy, J.J., Al-Muhtaseb, A.H., Zeaiter, J., 2019a. Hydrothermal carbonization of olive mill wastewater: liquid phase product. ⟨https://doi.org/10.1016/j.jece.2018.102833⟩.

Aunkor, M., Mahbubul, I., Saidur, R., Metselaar, H., 2016. RSC Adv. https://doi.org/10.1039/C6RA03189G.

Ayeda, L., Bouguerra, A., Charef, A., Bakhrouf, A., Mzoughi, R, E.L., 2019. Biodegradation of Olive Mill Wastewater by a newly isolated novel bacterial consortium under RSM. Optim. Cult. Cond. J. Water Proc. Eng. https://doi.org/10.1016/j.jwpe.2019.100986.

Aziz, F., El Achaby, M., Lissaneddine, A., Aziz, K., Ouazzani, N., Mamouni, R., Mandi, L., 2020. Composites with alginate beads: a novel design of nano-adsorbents impregnation for large-scale continuous flow wastewater treatment pilots. Saudi J. Biol. Sci. https://doi.org/10.1016/j.sjbs.2019.11.019.

Azzam, M.O.J., Al-Malah, K.I., Abu-Lail, N.I., 2004. Dynamic post-treatment response of olive mill effluent wastewater using activated carbon. J. Environ. Sci. Health Part A. https://doi.org/10.1081/ESE-120027383.

Azzaz, A.A., Jellali, S., Souissi, R., Ergaieg, K., Bousselmi, L., 2017. Alkaline-treated sawdust as an effective material for cationic dye removal from textile effluents under dynamic conditions: breakthrough curve prediction and mechanism exploration. Environ. Sci. Pollut. Res. ⟨https://link.springer.com/article/10.1007/s11356-017-9388-4⟩.

Bandosz, T.J., Block, K., 2006. Effect of pyrolysis temperature and time on catalytic performance of sewage sludge/industrial sludge-based composite adsorbents. https://doi.org//10.1016/j.apcatb.2006.04.006.

Benaddi, R., Aziz, F., harfi, K.E., Ouazzani, N., 2022. Column adsorption studies of phenolic compounds on nanoparticles synthesized from Moroccan phosphate rock. In: Heggy, E., Bermudez, V., Vermeersch, M. (eds.), Sustainable Energy-Water-Environment Nexus in Deserts. Advances in Science, Technology & Innovation. Springer, Cham. ⟨https://doi.org/10.1007/978-3-030-76081-6_13⟩.

Bertin, L., Ferri, F., Scoma, A., Marchetti, L., Fava, F., 2011. Recovery of high added value natural polyphenols from actual olive mill wastewater through solid phase extraction. Chem. Eng. J. doi: 10.1016/j.cej.2011.05.056.

Bhattacharya, G., Kandasamy, G., Soin, N., Upadhyay, R.K., Deshmukh, S., Maity, D., McLaughlin, J., Roy, S.S., 2017. RSC Adv. https://doi.org/10.1039/C6RA25630A.

Bouknana, D., Hammouti, B., Salghi, R., Jodeh, S., Zarrouk, A., 2014. Physicochemical Characterization of Olive Oil Mill Wastewaters in the eastern region of Morocco. ⟨https://doi.org/10.22159/jcr.2018v5i5.28840⟩.

Ceccon, L., Saccu, D., Procida, G., Cardinali, S., 2001. Liquid chromatographic determination of simple phenolic compounds in waste waters from olive oil production plants. J. AOAC Int. https://doi.org/10.1093/jaoac/84.6.1739.

Chittoo, B.S., Sutherland, C., 2019. Adsorption using lime-ironsludge–encapsulated calcium alginate beads for phosphate recoverywith ANN- and RSM-optimized encapsulation. J. Environ. Eng. https://doi.org/10.1061/(ASCE)EE.1943-7870.0001519.

Chkili, F., Abderrabba, M., 2015. Decontamination of olive mill wastewater with tow natural materials: sand and starch. J. Chem. Pharm. Res. ⟨https://www.jocpr.com/articles/decontamination-of-olive-mill-wastewater-with-tow-natural-materials-sand-and-starch.pdf⟩.

Coskun, T., Debik, E., Demir, N.M., 2010. Treatment of olive mill wastewaters by nanofiltration and reverse osmosis membranes. Desalination. https://doi.org/10.1016/j.desal.2010.04.034.

Dąbrowski, A., Podkościelny, P., Hubicki, Z., Barczak, M., 2005. Adsorption of phenolic compounds by activated carbon—a critical review. Chemosphere. https://doi.org/10.1016/j.chemosphere.2004.09.067.

Dehmani, Y., Ed-dra, A., Zennouhi, O., Bouymajane, A., Rhazi, F., Nassiri, L., & Abouarnadasse, S., 2020. Heliyon Chemical characterization and adsorption of oil mill wastewater on Moroccan clay in order to be used in the agricultural fi eld. Heliyon. ⟨https://doi.org/10.1016/j.heliyon.2020.e03164⟩.

Duarte, K.R., Justino, C., Panteleitchouk, T., Zrineh, A., Freitas, A.C., Duarte, A.C., Rocha-Santos, T.A.P., 2014. Removal of PCs in olive mill wastewater by silica-alginate-fungi biocomposites. Int. J. Environ. Sci. Technol. https://doi.org/10.1007/s13762-013-0268-2.

El Din Mahmoud, A., 2020. Eco-friendly reduction of graphene oxide via agricultural byproducts or aquatic macrophytes. Mater. Chem. Phys. https://doi.org/10.1016/j.matchemphys.2020.12.

El-Abbassi, A., Kiai, H., Raiti, J., Hafidi, A., 2014. Cloud point extraction of phenolic compounds from pretreated olive mill wastewater. Journal of Environmental Chemical Engineering. https://doi.org/10.1016/j.jece.2014.06.024.

Elayadi, F., Achak, M., Beniich, N., Belaqziz, M., El Adlouni, C., 2020. Factorial design for optimizing and modeling the removal of organic pollutants from olive mill wastewater using a novel low-cost bioadsorbent. Water, Air Soil Pollut. https://doi.org/10.1007/s11270-020-04695-8.

Ena, A., Pintucci, C., Carlozzi, P., 2012. The recovery of polyphenols from olive mill waste using two adsorbing vegetable matrices. J. Biotechnol. https://doi.org/10.1016/j.jbiotec.2011.06.027.

Freundlich, H.M.F., 1906. Über die adsorption in lösungen. Z. Phys. Chem. https://doi.org/10.1515/zpch-1907-5723.

Geim, A., Novoselov, K., 2007. The rise of graphene. Nat. Mater. https://doi.org/10.1142/9789814287005_0002.

Göktepeli, G., Yıldız, S., Yel, E., 2021. Phenol Adsorption on Magnetic Biochar Derived From Olive Pomace: Equilibrium, Kinetic and Thermodynamics. Hacettepe J. Biol. & Chem. https://doi.org/10.15671/hjbc.687387.

Gundogdu, A., Duran, C., Senturk, H.B., Soylak, M., Ozdes, D., Serencam, H., Imamoglu, M., 2012. Adsorption of phenol from aqueous solution on a low-cost activated carbon produced from tea industry waste: equilibrium, kinetic, and thermodynamic study. J. Chem. Eng. Data. https://doi.org/10.1021/je300597u.

Gupta, K., Khatri, O.P., 2017. Reduced graphene oxide as an effective adsorbent for removal of malachite green dye: plausible adsorption pathways. J. Colloid Interface Sci. https://doi.org/10.1016/j.jcis.2017.04.035.

Hameed, B., Rahman, A., 2008. Removal of phenol from aqueous solutions by adsorption onto activated carbon prepared from biomass material. J. Hazard. Mater. https://doi.org/10.1016/j.jhazmat.2008.03.028.

Haydari, I., Lissaneddine, A., Aziz, K., et al., 2022. Optimization of preparation conditions of a novel low-cost natural bio-sorbent from olive pomace and column adsorption processes on the removal of phenolic compounds from olive oil mill wastewater. Environ. Sci. Pollut. Res. https://doi.org/10.1007/s11356-022-20577-4.

He, H., Erpei, X., Zhanhong, Q., Tao, W., Shifang, W., Yuhua, L., Guannian, C., 2022. Phenol adsorption mechanism of organically modified bentonite and its microstructural changes. Sustainability. https://doi.org/10.3390/su14031318.

Ioannou-Ttofa, L., Michael-Kordatou, I., Fattas, S.C., Eusebio, A., et al., 2017. Treatment efficiency and economic feasibility of biological oxidation, membrane filtration and separation processes, and advanced oxidation for the purification and valorization of olive mill wastewater. Water Res. https://doi.org/10.1016/j.watres.2017.02.020.

Jagwani, D., Joshi, P., 2014. Deportation of toxic phenol from aqueous system by wheat husk. Int. J. Plant Anim. Environ. Sci. ⟨https://pdfs.semanticscholar.org/ea4a/1af9defb2b488c2ee0049a3b5e205c329a59.pdf⟩.

Jodra, Y., Mijangos, F., 2003. Phenol adsorption in immobilized activated carbon with alginate gels. Sep. Sci. Technol. https://doi.org/10.1081/SS-120019412.

Khadhri, N., Saad, M.E.K., Mosbah, M., ben, Moussaoui, Y., 2019. Batch and continuous column adsorption of indigo carmine onto activated carbon derived from date palm petiole. J. Environ. Chem. Eng. https://doi.org/10.1016/J.JECE.2018.11.020.

Kilic, M.Y., Abdelraheem, W.H., He, X., Kestioglu, K., Dionysiou, D.D., 2019. Photochemical treatment of tyrosol, a model phenolic compound present in olive mill wastewater, by hydroxyl and sulfate radical-based advanced oxidation processes (AOPs). J. Hazard. Mater. https://doi.org/10.1016/j.jhazmat.2018.06.062.

Kim, T.Y., Jin, H.J., Park, S.S., Kim, S.J., Cho, S.Y., 2008. Adsorption equilibrium of copper ion and phenol by powdered activated carbon, alginate bead and alginate-activated carbon bead. J. Ind. Eng. Chem. https://doi.org/10.1016/j.jiec.2008.07.004.

Kundu, S., Gupta, A.K., 2005. Analysis and modeling of fixed bed column operations on as (V) removal by adsorption onto iron oxide-coated cement. IOCC. J. Colloid Interface Sci. https://doi.org/10.1016/j.jcis.2005.04.006.

Langmuir, I., 1916. The constitution and fundamental properties of solids and liquids. Part-I. Solids. J. Am. Chem. Soc. https://doi.org/10.1021/ja02268a002.

Lawal, A.A., Hassan, M.A., Farid, M.A.A., Yasim-Anuar, T.A.T., Yusoff, M.Z.M., Zakaria, M.R., Shirai, Y., 2020. One-step steam pyrolysis for the production of mesoporous biochar from oil palm frond to effectively remove phenol in facultatively treated palm oil mill effluent. Environ. Technol. https://doi.org/10.1016/j.jclepro.2020.121643.

Li, J.M., Meng, X.G., Hu, C.W., Du, J., 2009. Adsorption of phenol, p-chlorophenol and p-nitrophenol onto functional chitosan. Bioresour. Technol. https://doi.org/10.1016/j.biortech.2008.09.015.

Lin, S.H., Juang, R.S., 2009. Adsorption of phenol and its derivatives from water using synthetic resins and low-cost natural adsorbents: a review. J. Environ. Manag. https://doi.org/10.1016/j.jenvman.2008.09.003.

Lissaneddine, A., Mandi, L., El, M., Mousset, E., Rene, E.R., Ouazzani, N., & Aziz, F., 2021. Chemosphere Performance and dynamic modeling of a continuously operated pomace olive packed bed for olive mill wastewater treatment and phenol recovery. ⟨https://doi.org/10.1016/j.chemosphere.2021.130797⟩.

Liu, X., Xu, J., Zhao, Y., Shi, H., Huang, C.H., 2019. Hydrophobic sorption behaviors of 17B-Estradiol on environmental microplastics. Chemosphere. https://doi.org/10.1016/j.chemosphere.2019.03.162.

Lopez-Ramon, M.V., Stoeckli, F., Moreno-Castilla, C., Carrasco-Marin, F., 1999. On the characterization of acidic and basic surface sites on carbons by various techniques. Carbon. https://doi.org/10.1016/S0008-6223(98)00317-0.

Mahmoud, A.E.D., Hosny, M., El-Maghrabi, N., et al., 2022. Facile synthesis of reduced graphene oxide by Tecoma stans extracts for efficient removal of Ni (II) from water: batch experiments and response surface methodology. Sustain. Environ. Res. https://doi.org/10.1186/s42834-022-00131-0.

Mohd Din, A.T., Hameed, B.H., Ahmad, A.L., 2009. Batch adsorption of phenol onto physiochemical-activated coconut shell. J. Hazard. Mater. ⟨https://doi.org/10.1016/j.jhazmat.2008.05.009⟩.

Mojoudi, N., Mirghaffari, N., Soleimani, M., Shariatmadari, H., Belver, C., Bedia, J., 2019. Phenol adsorption on high microporous activated carbons prepared from oily sludge: equilibrium, kinetic and thermodynamic studies. Sci. Rep. 9, 19352. https://doi.org/10.1038/s41598-019-55794-4.

Moon, I.K., Lee, J., Ruof, R.S., Lee, H., 2010. Reduced graphene oxide by chemical graphitization. Nat. Commun. https://doi.org/10.1038/ncomms1067.

Nadavala, S.K., Swayampakula, K., Boddu, V.M., Abburi, K., 2009. Biosorption of phenol and o-chlorophenol from aqueous solutions on to chitosan-calcium alginate blended beads. J. Hazard. Mater. https://doi.org/10.1016/j.jhazmat.2008.05.070.

Njimou, R.J., Godwin, J., Pahimi, H., Maicaneanu, S.A., et al., 2021. Biocomposite spheres based on aluminum oxide dispersed with orange-peel powder for adsorption of phenol from batch membrane fraction of olive mill wastewater. Colloids Interface Sci. Commun. https://doi.org/10.1016/j.colcom.2021.100402.

Paraskeva, C.A., Papadakis, V.G., Kanellopoulou, D.G., Koutsoukos, P.G., Angelopoulos, K.C., 2007. Membrane filtration of olive mill waste-water and exploitation of its fractions. Water Environ. Res. https://doi.org/10.2175/106143006X115345.

Patel, H., 2019. Fixed-bed column adsorption study: a comprehensive review. Appl. Water Sci. https://doi.org/10.1007/s13201-019-0927-7.

Rocha, P.D., Franca, A.S., Oliveira, L.S., Preparation, A.A., 2015. Batch and Column Studies of Phenol Adsorption by an Activated Carbon Based on Acid Treatment of Corn Cobs. ⟨https://doi.org/10.7763/IJET.2015.V7.837⟩.

Rout, D.R., Jena, H.M., 2022. Synthesis of novel epichlorohydrin cross-linked β-cyclodextrin functionalized with reduced graphene oxide composite adsorbent for treatment of phenolic wastewater. Environ. Sci. Pollut. Res. https://doi.org/10.1007/s11356-022-21018-y.

Singleton, V.L., Rossi, J.A., 1965. Colorimetry of total phenolics with phosphomolybdic-phosphotungstic acid reagents. Am. J. Enol. Vitic. http://www.ajevonline.org/content/16/3/144.full.pdf+html.

Subramanyam, B., Das, A, A., 2009. Linearized and non-linearized isotherm models comparative study on adsorption of aqueous phenol solution in soil. Int. J. Environ. Sci. https://doi.org/10.1007/BF03326104.

Sun, J., Liu, X., Zhang, F., Zhou, J., Wu, J., Alsaedi, A., Li, J., 2019. Insight into the mechanism of adsorption of phenol and resorcinol on activated carbons with different oxidation degrees. Colloid Surf. Physicochem. Eng. Asp. https://doi.org/10.1016/j.colsurfa.2018.11.042.

Tahermansouri, H., Dehghan, Z., Kiani, F., 2015. Phenol adsorption from aqueous solutions by functionalized multiwalled carbon nanotubes with a pyrazoline derivative in the presence of ultrasound. RSC Adv. https://doi.org/10.1039/C5RA02800K.

Thawornchaisit, U., Pakulanon, K., 2007. Application of dried sewage sludge as phenol biosorbent. Bioresour. Technol. https://doi.org/10.1016/j.biortech.2005.11.004.

Vavouraki, A.I., Dareioti, M.A., Kornaros, M., 2020. Olive mill wastewater (OMW) polyphenols adsorption onto polymeric resins: Part I-batch anaerobic digestion of OMW. Waste Biomass Valoriz. https://doi.org/10.1007/s12649-020-01168-1.

Ververi, M., Goula, A.M., 2019. Pomegranate peel and orange juice by-product as new biosorbents ofphenolic compounds from olive mill wastewaters. Chem. Eng. Process. doi: 10. 1016/j.cep.2019.03.010.

Vuppala, S., Shaik, R.U., 2021. applied sciences Multi-Response Optimization of Coagulation and Flocculation of Olive Mill Wastewater: Statistical Approach. ⟨https://doi.org/10.3390/app11052344⟩.

Weber, W.J., Morris, J.C., 1963. Kinetics of adsorption on carbon from solution. J. Sanit. Eng. Div. Am. Soc. Civ. Eng. https://doi.org/10.1061/JSEDAI.0000430.

Weng, X.L., Wu, J., Ma, L., Owens, G., Chen, Z.L., 2019. Impact of synthesis conditions on Pb (II) removal efficiency from aqueous solution by green tea extract reduced graphene oxide. Chem. Eng. J. https://doi.org/10.1016/j.cej.2018.11.089.

Yuney, K., Oladipo, A.A., Gazi, M., Younis, D.Z., 2020. Chemosphere CuO coated olive cake nanocomposites for rapid phenol removal and effective discoloration of high strength olive mill wastewater. Chemosphere. https://doi.org/10.1016/j.chemosphere.2020.126703.

Zaharaki, D., Komnitsas, K., 2018. Existing and Emerging Technologies for the Treatment of Olive Oil Mill Wastewaters. Department of Mineral Resources Engineering, Technical University of Crete, Hania, Greece. ⟨http://purl.tuc.gr/dl/dias/329A832D-22A8-406F-9D03-5885E0A0C0A8⟩.

Zefzoufi,M. Fdil, R., Bouamama, H., Gadhi, C., Kartakura, Y., Mouzdahir, A., Sraidi, K., 2021. Effect of extracts and isolated compounds derived from *Retama monosperma* (L.) Boiss. on anti-aging gene expression in human keratinocytes. J. Ethnopharmacol., 280, 2021. ⟨https://doi.org/10.1016/j.jep.2021.114451⟩.